Biogeochemical processes accounting for the natural mercury variations in the Southern Ocean diatom ooze sediments

Sara Zaferani[1], Harald Biester[1]

[1]Institut für Geoökologie AG Umweltgeochemie, Technische Universität Braunschweig, Braunschweig, 38106, Germany

Correspondence to: Sara Zaferani (s.zaferani@tu-braunschweig.de)

Abstract. Due to its toxic nature and its high potential for biomagnification, mercury is a pollutant of concern. Understanding the marine biogeochemical cycle of mercury is crucial as consumption of mercury enriched marine fish is the most important pathway of human exposure to monomethylmercury, a neurotoxin. However, due to the lack of long-term marine records, the role of the oceans in the global mercury cycle is poorly understood. We do not have well-documented data of natural mercury accumulations during changing environmental conditions, e.g. sea surface conditions in the ocean. To understand the influence of different sea surface conditions (climate-induced changes in ice coverage and biological production) on natural mercury accumulation, we used a continuous ~ 170 m Holocene biogenic sedimentary record from Adélie Basin, East Antarctica, which mainly consists of silica-based skeletons of diatoms. We performed Principal Component Analysis and regression analysis on element concentrations and corresponding residuals, respectively to investigate the link between sediment mercury accumulation, terrestrial inputs, and phytoplankton productivity. Preindustrial mercury in the remote marine basin shows extremely high accumulation rates (median: 556 µg m^{-2} yr^{-1}) that displayed periodic-like variations. Our analyses show that the variations in total mercury concentrations and accumulation rates are associated with biological production and related scavenging of water phase mercury by rapidly sinking algae or algae-derived organic matter after intense algae blooms. High accumulation rates of other major and trace elements further reveal that in regions of high primary productivity, settling of biogenic materials removes a large fraction of dissolved or particulate bound elements from free water phase through scavenging or biological uptake. The link between mercury cycling and primary production will need to be considered in future studies of the marine mercury cycle under primary production enhancement through climatic, temperature, and nutrient availability changes.

1 Introduction

Mercury (Hg) is a metal of environmental concern due to its ability to be transported through the atmosphere from industrial point sources to remote regions and its transformations into highly bioaccumulative and neurotoxic methylated forms. In the

27 global biogeochemical cycle of Hg, the ocean, as the dominant physical feature of our planet Earth, is of specific concern. A

28 substantial amount of Hg (~ 80 %) which is emitted to the atmosphere from natural and anthropogenic sources reaches the

29 ocean (Horowitz et al., 2017; Schartup et al., 2019) and ocean sediments are considered to be the ultimate sink of Hg on a

30 timescale of tens of thousands of years (Fitzgerald et al., 2007; Selin, 2009; Amos et al., 2013). Despite the important role of

31 marine sedimentation in the global Hg biogeochemical cycle, little is known about the rates or amount of Hg accumulation in

32 marine sediments, especially in the open ocean. In contrast to the well-studied Hg cycling in terrestrial environments,

33 knowledge about the temporal and spatial distribution of Hg in the marine environment is limited to model estimations (Mason

34 and Sheu, 2002; Sunderland and Mason, 2007), water column measurements (Cossa et al., 2011; Lamborg et al., 2014; Canário

35 et al., 2017), and very few sediment measurements (Kita et al., 2013; Aksentov and Sattarova, 2020). A main reason for our

36 limited understanding of the fate of Hg in the oceans is the lack of high resolution marine sedimentary records, especially from

37 the deep ocean (Zaferani et al., 2018).

38 Hg input to the ocean is primarily through atmospheric deposition (Mason et al., 1994; Driscoll et al., 2013). After deposition,

39 as either mercuric ion (Hg^{2+}) or elemental Hg (Hg^0), Hg can be reduced to Hg^0 and evaded to the atmosphere, or scavenged

40 from the water column by particulate matter and eventually buried in deep-sea sediments (Mason et al., 2012; Lamborg et al.,

41 2014). Most marine surface waters are believed to be close to equilibrium between Hg deposition and evasion or saturated in

42 Hg^0 due to biologically mediated (Mason et al., 1995; Rolfhus and Fitzgerald, 2004; Whalin et al., 2007) and photochemical

43 reduction (Amyot et al., 1997; Mason et al., 2001) followed by re-emission of Hg^0 to the atmosphere. It has been estimated

44 that almost 96 % of the deposited Hg to the ocean is lost through evasion from the surface, and only 30 % of the Hg flux that

45 reaches the deep ocean is preserved in sediments (Mason and Sheu, 2002). However, other studies indicate that the ocean

46 surface waters become a sink for atmospheric Hg at the high nutrient levels and related high primary productivity (Soerensen

47 et al., 2016).

48 There are contradictory statements about the Hg deposition and evasion to/from different surface waters. Early works suggest

49 that Hg evasion is high in productive upwelling regions of the ocean due to enhanced biological reduction (Fitzgerald et al.,

50 1984; Mason and Fitzgerald, 1993). More recent studies, with higher spatial and temporal resolutions, suggest lower Hg

51 evasion in productive regions (O'Driscoll et al., 2006; Qureshi et al., 2010; Soerensen et al., 2013; Soerensen et al., 2014).

52 Measurements of Hg from these recent studies show relatively low concentrations of atmospheric and surface water phase Hg^0

53 in regions with high productivity compared to areas with lower productivity. These studies related their observation to sorption

54 and scavenging of Hg by suspended organic particles. They suggested that removal of Hg^{2+} associated with sorption and

55 scavenging by suspended organic particles in productive regions reduces the amount of available Hg^{2+} for reduction and re-

56 emission. Therefore applying the model estimates across the entire ocean introduces substantial uncertainty and one area in

particular that highlights this uncertainty is the underestimation of the role of biological productivity as a major vector of Hg sedimentation in the oceans.

The marine biogeochemical cycle, especially sedimentation of many elements (Fowler and Knauer, 1986; Morel and Price, 2003; Schlesinger and Bernhardt, 2013), including Hg (Kita et al. 2013; Lamborg et al., 2016; Zaferani et al., 2018), in the ocean is controlled directly and indirectly by biological productivity. Biogenic particles control the distribution of elements through primary production, sinking, and decomposition (Fowler and Knauer, 1986). Besides direct uptake across cell membranes through active metabolism, phytoplankton and sinking biogenic particles can scavenge and remove many other elements from the dissolved phase and transport them to the deep sea. Sinking speed of biogenic particles plays an important role in the final fate of those elements. Rapidly sinking particles such as diatom agglomerates transfer elements to the deep sea (Fowler and Knauer, 1986; Smetacek et al., 2012), whereas elements associated with the slowly sinking particulates will release back to the water phase through remineralization (Fowler and Knauer, 1986). In areas where pronounced seasonal blooms take place, phytoplankton species appear to reach the deep-sea floor relatively fast and intact. Seasonal blooms in the surface waters will also cause temporally variable fluxes of elements in the deep ocean (Fowler and Knauer, 1986; Michel et al., 2002; Pilskaln et al., 2004). For Hg, these findings are supported by water column (Lamborg et al., 2014) and marine sediment measurements (Kita et al., 2013; Aksentov and Sattarova, 2020). Lamborg et al. (2014) described a nutrient-like distribution of Hg in the water column of oceans. This study indicates that similar to carbon (C) and phosphorus (P), Hg shows higher concentrations in the deep water due to its release during organic matter decomposition. Kita et al. (2013) found a positive correlation between Hg and the absolute abundance of phytoplankton species in sediments of the Caribbean Sea. Hg in these sediments was assumed to be a result of Hg binding by phytoplankton depositing Hg-bearing organic matter in the photic zone. A similar conclusion was reached by Aksentov and Sattarova (2020) who used a thermo-scanning technique to detect Hg forms. They found that biological productivity controlled the Hg burial in Northwest Pacific bottom sediments and that the forms of Hg depended on the diatom content.

These observations can be due to Hg—phytoplankton interactions and up-take or binding of Hg from the water by phytoplankton (Le Faucheur et al., 2014; Mason et al., 1996). This interaction controls the flux of Hg from the water column to sediments and facilitates the downward flux of Hg to the seafloor (Soerensen et al., 2014; Soerensen et al., 2016; Lamborg et al., 2016; Zaferani et al., 2018), which, as mentioned, has traditionally been considered to be slow in its nature. Thus, underestimating the role of biological productivity in the marine biogeochemical cycle of Hg may lead to an overestimation of re-emission fluxes from surface water and an underestimation of the Hg flux to deep-sea sediments.

In this context, the Southern Ocean is of particular interest due to its high concentrations of nutrients and related elevated primary productivity (Arrigo et al., 1998). In the Southern Ocean, diatoms are major primary producers (Crosta et al., 2005).

87   Their siliceous cell walls preserve well in sediments and form diatom ooze (Fütterer, 2006). The sedimentation rate of diatom

88   ooze is high, estimated to reach up to 2 cm yr^{-1} (Escutia et al., 2011), making diatom ooze deposits around Antarctica a unique

89   geochemical archive to study the influence of primary productivity as well as natural and anthropogenic changes on the marine

90   biogeochemical cycle of Hg.

91   Despite providing a unique geochemical archive, studies on Hg cycling in the Southern Ocean, particularly in the Antarctic

92   region, are generally limited to water column (Cossa et al., 2011; Nerentorp Mastromonaco et al., 2017b; Canário et al., 2017),

93   surface water/air (Nerentorp Mastromonaco et al., 2017a; Wang et al., 2017), and ice core analyses (Vandal et al., 1993). Cossa

94   et al. (2011) showed a nutrient-like distribution of Hg in water column that ranged between 0.6 and 2.8 pmol L^{-1}. Nerentorp

95   Mastromonaco et al. (2017b) found higher total Hg concentration than Cossa et al. (2011) with no significant vertical

96   variations. Both studies reported seasonal variations in Hg concentrations and related them to seasonal variations of

97   atmospheric Hg deposition (Cossa et al., 2011; Nerentorp Mastromonaco et al., 2017b) as well as the Hg inputs from melting

98   sea ice and snow (Nerentorp Mastromonaco et al, 2017b). Total Hg concentrations in the Atlantic sector of the Southern Ocean

99   obtained during a study by Canário et al. (2017) were also, in general, comparable to those obtained by Cossa et al. (2011)

100 except for some stations that showed higher total Hg concentrations. Canário et al. (2017) attributed these differences to the

101 different stages of phytoplankton bloom during the sampling. This led to lower dissolved Hg in water in the middle-end stage

102 of the bloom compare to the beginning stage of the bloom, owing to the Hg uptake by phytoplankton (Canário et al. 2017).

103 Measurements of gaseous elemental mercury (GEM) and dissolved gaseous mercury (DGM) in surface water showed spatial

104 and seasonal variations as well (Nerentorp Mastromonaco et al., 2017a; Wang et al., 2017). These studies related the increase

105 of DGM and GEM concentrations to the presence and absence of sea ice. Sea ice that could prevent Hg evasion to the

106 atmosphere, could initially lead to an increase in Hg emissions to the atmosphere when diminishing. Hg concentrations in an

107 ice core covering the past 34 Kyr, varied between 0.0005 and 0.0021 µg kg^{-1}, corresponding to depositional fluxes of 0.009

108 and 0.031 µg m^{-2} yr^{-1} during the Holocene and the Last Glacial Maximum, respectively (Vandal et al., 1993). Vandal et al.

109 (1993) attributed the observed enhanced Hg flux during colder periods to marine biological productivity and emissions of

110 volatile Hg compounds from the ocean. Given the different results of the existing studies point to the gaps in our understanding

111 of Hg behavior in productive remote areas which warrants further investigation in the Southern Ocean.

112 In a previous paper, we discussed the accumulation of anthropogenic Hg in sediments of Adélie Basin, offshore East

113 Antarctica. The ~ 2-fold increase in Hg concentrations and accumulation rates in the upper ~ 2.80 m depth of the core was

114 attributed to the onset of the industrial revolution and the strong increase in coal burning at ~ 1850 CE (Zaferani et al., 2018).

115 Here, we discuss the natural processes (e.g. changes in biogenic and terrestrial material fluxes) that controlled Hg accumulation

116 in the same sediment core prior to 1850 CE throughout the past 8600 years. We investigated a continuous ~ 170 m long

117 Holocene laminated diatom ooze sediment record from the Adélie Basin. Covering almost the entire Holocene, the core allows

118   the determination of natural variations of Hg accumulation rates in these sediments prior to major anthropogenic influences.

119   Our main objective was to investigate the influence of different Hg sources, climate-induced changes in biological productivity

120   and terrestrial fluxes (through melting of glacier ice), which have controlled the sequestration of Hg in these sediments. To

121   evaluate the influence of different biogeochemical processes on the Hg accumulation in sediments, with an emphasis on the

122   role of changes in planktonic productivity, we combined the data on Hg accumulation with data derived from multi-element

123   analyses.

124

2. Materials and methods

2.1 Study site and core collection

127   Sediments of the Adélie Basin were collected during the Integrated Ocean Drilling Program (IODP) Expedition from hole

128   U1357B 318 in 2010. U1357B is located on the continental shelf off Wilkes Land at the Mertz Glacier polynya (region of

129   open water surrounded by sea ice), Antarctica (66°24.7990′ S, 140°25.5705′ E) at about 1021.5 m water depth (Escutia et al.,

130   2011) (Fig 1). The total length of the recovered core is 170.7 m, corresponding to nearly the entire Holocene (Escutia et al.,

131   2011). The core was sliced by 5cc plastic scoops to 1 cm slices. Samples in the upper core (3.2–25.05 mbsf) were taken at ~

132   40 cm intervals (a resolution of ~ 20 years) and ~ 400 cm intervals (a resolution of ~ 200 years) in deeper sections (25.05–

133   170.35 mbsf), resulting in a total of 78 samples. Age data and age model (which is based on Compound-specific ^{14}C dating)

134   were obtained from Yamane et al. (2014).

135   The sediment core is characterized by light and dark laminations which are undisturbed by sea-level changes or glacial erosion

136   (Denis et al., 2006; Escutia et al., 2011). Light laminations correspond to spring seasons when light and high nutrient levels

137   promote intense phytoplankton blooms and are mainly composed of biogenic materials (mostly diatom with minor abundance

138   of silicoflagellates, sponge spicules, radiolarians, and foraminifers). Dark layers correspond to the summer/autumn season

139   when sea ice has retreated, and nutrient levels are low. Dark laminations are composed of a mixture of biogenic and terrigenous

140   materials resulting from summer production in open water, with glacial and subglacial inputs, respectively. High levels of

141   primary production in surface water of this region, coupled with rapid fluxes of biogenic debris directly to the seafloor, led to

142   high sedimentation rates of up to 2.0 cm yr^{-1} during the past 10,000 years (Escutia et al., 2011).

2.2 Analyses of mercury and major and trace metals

144   All samples were freeze-dried and ground using a glass pestle prior to geochemical analysis. Total Hg was determined by

145   thermal decomposition followed by pre-concentration of Hg on a gold trap and CVAAS Hg detection using a Milestone DMA-

146 80 analyzer (US EPA Method 1998). The quality of the analysis was ensured by including a certified reference material (CRM)

147 (Canmet LKSD-4 = 190 ± 17 ng g^{-1}) alongside the analyzed samples. The average measured concentration for LKSD-4 was

148 197 ± 11 ng g^{-1}. Replicate analyses (n = 20) were always within an RSD of 10 % of the certified value.

149 The samples were analyzed for concentrations of silicon (Si), titanium (Ti), zirconium (Zr), sulfur (S), calcium (Ca), potassium

150 (K), aluminum (Al), yttrium (Y), manganese (Mn), strontium (Sr), iron (Fe), lead (Pb), copper (Cu), zinc (Zn), arsenic (As),

151 bromine (Br), nickel (Ni), chlorine (Cl), and rubidium (Rb) by energy dispersive X-ray fluorescence (ED-XRF). The

152 calibration method, accuracy, and precision are described in detail in Cheburkin and Shotyk (1996). The CRMs (Canmet

153 LKSD-4, NRC/CNRC-PACS-2, NRC/CNR-Mess-3, and NCS-DC75304) and replicates were measured in each set of samples

154 for accuracy and precision control. Repeated analysis of CRMs gave relative standard deviation (SRD) less than 10 % for Si,

155 Al, Ca, Y, Sr, Zr, Br, and Rb, 6–15 % for Ti, K, Zn, S, Fe, Mn, and Pb, 6–19 % for Cl, 10–20 % for Ni, 9–14 % for Cu, and

156 14–22 % for As.

157 **2.3 Statistical analyses**

158 Principal component analysis (PCA) was applied to the major and trace element concentrations to identify processes

159 controlling the variability of elements in the sediments. When there is a complex set of variables, PCA is used to reduce a large

160 number of variables to a new set of artificial variables, called principal components. Each component includes variables with

161 a similar down core pattern. The principal components are then interpreted in terms of relevant geochemical processes that can

162 control the variability of the major and trace elements in the sediments. The derived interpretation from PCA was then

163 combined with the Hg data to examine the processes that could affect Hg accumulations. The analysis was performed on the

164 standardized concentration data using Z-scores (expressed in terms of standard deviations from their means). Regressions

165 analysis of the corresponding residuals was used to establish relationships between the abundance of elements, by considering

166 Si concentration as an independent variable and other element concentrations as dependent variables. Correlation analysis and

167 PCA were performed using the statistical software SPSS 25.0.

168 **3. Results and discussion**

169 **3.1 Geochemical processes controlling the distribution of the elements in the sediments**

170 Concentration profiles and accumulation rates of Si, Al, K, Ti, S, Ca, Zn, Fe, Br, As, and Cl are shown in Fig. 2-5. The

171 preindustrial geochemical record of Adélie Basin sediments is generally characterized by periodic-like variations in the relative

172 abundance of major and trace elements. The records of element accumulation rates largely follow those of periodic-like

173 variations of concentrations and show no significant trend with depth (except Cl).

174 Si has the highest concentration of all elements in the sediments. On one hand, Si is associated with the flux of terrestrial

175 derived mineral components and on the other hand with siliceous phytoplankton, protozoans, protists, plant phytoliths, and

176 sponge spicules (Croudace and Rothwell, 2015). Si is mainly biogenic in origin in Adélie Basin sediments, dominated by

177 diatoms (Escutia et al., 2011), and contribution of terrigenous Si is low. Therefore, it is used as a proxy for diatom abundance.

178 The record of Si concentrations shows periodic-like variations by a factor of ~ 2 between 21 % and 50 %, with a median of 33

179 %, corresponding to 70 % SiO_2 or biogenic silica. Concentrations of Al, K, and Ti (as indicators of changes in the flux of

180 lithogenic materials) range between ~ 1.6–7.3 %, ~ 0.37–1.11 %, and ~ 716–1778 mg kg^{-1}, respectively. S and Ca

181 concentrations, which are associated with the biogenic productivity, vary between ~ 0.13–0.87 % and 0.72–1.49 %,

182 respectively. Ca concentration indicates that calcite producing microorganisms are of minor importance in the Adélie Basin.

183 Concentration of Zn, an important micronutrient for marine phytoplankton (Morel et al., 1994), ranges between ~ 96 and 216

184 mg kg^{-1}. Fe is another essential micronutrient for marine primary production (Smetacek et al., 2012) and biochemical processes

185 of phytoplankton such as photosynthesis, respiration, and nitrogen fixation (Lohan and Tagliabue, 2018). Concentration of Fe

186 varies between ~1.05 and 3.46 %, which is similar to other siliceous sediments but lower than the reported concentration in

187 other ocean sediments (Chen et al., 1996). Fe concentrations increase at 66.45 m depth to the top of the core by a factor of ~

188 1.6 (from a median of ~ 1.50 % below the 66.45 m depth to ~ 2.40 % above the 66.45 m depth). This is attributed to the upward

189 transport of Fe under anoxic conditions. Chlorine was found to be another major component in these sediments. Cl can go

190 through biological pathways (incorporation into algae) and reach the sediments by the fast-sinking detritus (Leri et al., 2015).

191 Concentrations vary between ~ 1.3 and 19 %, with a median of median 4.5 %, and show a decrease from the top to the bottom

192 of the core which is likely attributed to the increasing mineralization of organic matter with age and the release of chloride

193 through reductive dechlorination.

194 The PCA resulted in five components, explaining almost 82 % of the total variance (Table 1). The first component (Cp1),

195 explains 33 % of the variance and shows large (> 0.7) positive loadings of Mn, Ti, Rb, Zr, K, and Y and moderate positive

196 loading of Fe. The second component (Cp2), which explains 20 % of the variance, is characterized by large positive loadings

197 of Al, Si, S, and Cl and moderate positive loading of K and Ca. The third component (Cp3) explains 17 % of the variance and

198 shows large positive loadings of Zn, Cu, and Ni and moderate positive loading of Fe. The fourth and fifth components (Cp4

199 and Cp5) account for 7 and 5 % of the variance, respectively. Cp4 is characterized by high positive loadings for Hg and As

200 and moderate negative loading of Pb. Cp5 shows positive loadings for Sr and Ca.

201 In general, results of PCA imply that opening and closing of the polynya and biological production are the most important

202 factors influencing sedimentation in the Adélie Basin. This has been shown by loadings of elemental proxies for terrigenous

203 and biological material inputs. Briefly, Cp1, which includes positive loadings of lithogenic elements, represents the variability

204 of terrigenous inputs. Melting of ice releases trapped lithogenic material into the water and leads to the sinking of lithogenic

205 particles and their sedimentation. Cp2 comprises loadings of elements of both biogenic and terrigenous sources. This

206 component appears to reflect phytoplankton blooms and export of biological materials. After ice melt, when the ice is opening,

207 favorable conditions for biological productivity lead to phytoplankton blooms and export of biogenic materials to the seafloor

208 (Denis et al., 2006). Biogenic material is mainly opal because diatoms are a major component of blooms in the Adélie Basin

209 (Escutia et al., 2011). The sinking of diatoms from the surface and their sedimentation can cause scavenging of elements during

210 bloom time. Al shows positive loadings in this component rather than in Cp1. This, other than association with the flux of

211 aluminosilicates material can also be attributed to the scavenging of Al by diatom particles (Moran and Moore, 1992). Cl also

212 shows loading in Cp2. The possible explanation for the observed covariation is that marine phytoplankton is rich in

213 polyunsaturated lipids and can account as chlorination substrates (Leri et al., 2015). However, the organic C content of Adélie

214 Basin sediments is generally low (between 1 and 2 wt %), and we hypothesis that some of the Cl must be in an inorganic form

215 trapped in sediments owing to high sedimentation rates. Cp3 is mainly characterized by elements that are associated with the

216 organic fraction of diatom cells. This component appears to reflect the remineralization process like decomposition of organic

217 particles during sinking. Trace elements associated with organic parts of cells can be released back into the water column

218 during decomposition. Therefore, cellular locations of elements, i.e. opal frustules of diatoms or organic matter of diatom cells,

219 created different components of Cp2 and Cp3. Cp4 consists of organic particle reactive metals, e.g. Hg and Pb. The possible

220 explanation for not having these two particle reactive metals in Cp2 is that some of these two metals begin to enter the system

221 after ice melting, while Cp2 shows scavenging of elements by diatoms that are already present in the water column. Since Pb

222 and Hg are negatively correlated, this component cannot reflect a pollution signal. The reason for that could be the

223 characteristic of Pb that decreases its impact in remote areas such as Antarctica. Atmospheric Pb is associated with particles

224 and therefore is rapidly removed by wet and dry deposition. Moreover, Southern Ocean circumpolar vortex that isolates

225 Antarctica from the other continental landmasses in the Southern Hemisphere will further limit Pb transport to Antarctica.

226 Covariation of Ca and Sr in Cp5 represents sedimentation of planktonic foraminifera, which appears to be of minor importance

227 here.

228 Cp1 explains 33 % of the variance and accounts for much of the variability/process which controlled the geochemical

229 composition of these sediments. However, the high concentration of Si and low concentrations of terrigenous elements imply

230 that in an environment like Adélie Basin, with extremely high productivity, input of lithogenic materials is changing while

231 different diatom taxa are always present in the system, e.g. as sea ice-associated and open ocean diatom (Escutia et al., 2011).

232 It has been shown before that seasonal blooms in ocean surface waters result in temporary variable fluxes of elements to the

233 deep ocean (Fowler and Knauer, 1986; Michel et al., 2002; Pilskaln et al., 2004). Although the core was not sampled at a one-

234 year resolution in our study, we suggest that the fluctuations of elemental concentrations are likely related to the seasonal

235 blooms and variation of sea surface conditions like ice melting and freezing and its subsequent biological or terrestrial materials

exports. Sampling in light (associated with spring) or dark (associated with summer/autumn) laminae, which contains different amounts of biogenic or terrestrial materials can cause the observed variations (see Sect. 2.1).

The element concentrations are comparable to other published sediment data, while the accumulation rates are much higher than other reported values. The existence of rapidly settling particles in the Adélie Basin can explain the high element accumulation rates. When nonessential elements and essential elements show high accumulation rates, it is tempting to suggest that most elements in the water column of Adélie Basin are subjected to removal by intense phytoplankton blooms through consumption or scavenging. This agrees with the study of Fowler and Knauer (1986) that demonstrated the role of large particles in the transport of elements through the oceanic water column. Aggregation of diatoms, which creates large particles (Turner, 2015), sink to the seafloor and can create a space in which elements can be trapped (Shanks and Trent, 1979). This enhances removal of elements from the water column and their sedimentation as well.

3.2 Holocene record of mercury concentrations and accumulation rates

In the preindustrial period, i.e. from the bottom of the core at ~ 170 m to 2.80 m depth (8600 years ago to ~ 1850 CE), the Hg record shows no obvious trend with depth but rather periodic-like variations. Hg concentrations fluctuate by a factor of about 2 between 12.6 and 21.1 µg kg^{-1} within 170–137 m depth and between 21.7 and 44.6 µg kg^{-1} within 137–2.80 m depth of the core, with two more pronounced peaks at around 9.99 and 8.20 m depth (Fig. 2 and 3). The lower concentration of Hg within 170–137 m depth of the core is probably attributed to cooler conditions in Adélie Basin (Crosta et al., 2007) and sea ice cover during this period. Hg accumulation rates in the preindustrial period (Fig. 4 and 5) largely follow the Hg concentration record, with periodic-like variations and a median of 556 µg m^{-2} yr^{-1}, which largely surpass the reported Hg deposition rates to the oceans (Mason and Sheu, 2002).

The high preindustrial Hg accumulation rates in Adélie Basin sediments cannot be explained by preindustrial atmospheric Hg depositions alone, which did not exceed 20 µg m^{-2} as recorded in an Antarctic ice core (Vandal et al., 1993). Therefore, non-atmospheric sources, such as dissolved water phase Hg or terrestrial inputs, are needed for the observed high Hg enrichment in these sediments.

To identify driving forces behind the variations in Hg accumulation we used our PCA results. PCA demonstrated that two main processes, i.e. biogenic productivity and lithogenic inputs, controlled the flux of elements to Adélie Basin sediments. The component scores, which illustrate the depth dependency of the extracted components, are characterized by see-saw patterns throughout the entire core. This indicates different contributions of biogenic and terrigenous inputs most likely associated with spring and summer/autumn seasons, respectively.

264 The variance of Hg was not captured by Cp1, Cp2, or Cp3. Hg instead forms a group on Cp4 together with positive loading of
265 As and negative loading of Pb. The absence of significant loading of Hg on Cp1, Cp2, and Cp3 (Table 1) and the lack of
266 similarity between component scores and Hg concentrations (Fig. 6 and 7), in the preindustrial period, indicates that Hg fluxes
267 are not significantly influenced by changes in lithogenic inputs through ice melting. These results further indicate that changes
268 in the contribution of biogenic material can not explain the variation in Hg accumulation in the sediments.

269 Although the high Hg accumulation rates observed in the Adélie Basin sediments could not be explained by atmospheric Hg
270 deposition, but we expect that the Hg flux from the atmosphere will probably increase during algae blooms attributed to the
271 removal of dissolved Hg through scavenging by algae. Hg removal from the upper water column by diatom organic matter
272 will also likely decrease Hg re-evasion to the atmosphere as previously assumed in model studies (Soerensen et al., 2014;
273 Soerensen et al., 2016).

274 We have hypothesized that the high Hg enrichment in Adélie Basin sediments has been caused by scavenging of dissolved
275 water phase Hg by a large amount of fast sinking algal debris. To proof this hypothesis we calculated the maximum amount
276 of Hg which could be scavenged by a single bloom event using the Hg concentration of 271 ± 78 pg L^{-1} in Antarctic Bottom
277 Water, as determined by Cossa et al. (2011). The amount of Hg in a water column of one m^2 and 1000 m depth would then
278 amount to 271 ± 78 µg. This means that only about 2-3 algae blooms and scavenging events per year are necessary to obtain
279 the average Hg accumulation rate in Adélie Basin diatom ooze sediments, i.e. 556 ± 137 µg m^{-2} yr^{-1}. This appears to be likely
280 taking into account that bloom events are frequent during Antarctic summer and that the sinking speed of diatom agglomerates
281 at Adélie Basin is high (100-400 m per day) (Jansen et al., 2018). The annual cycle of water mass transformation beneath the
282 Mertz Glacier polynya system (Williams et al., 2008) and the exchange of water masses can rapidly "refill" the Hg inventory
283 in the water column after a scavenging event. While algal bloom is a local event at the surface water of the Adèlie Basin, the
284 exchange of water masses, which have not been affected by algae blooms, could refill the Hg inventory in the water column
285 (Fig. 8).

286 The main reason for not finding any statistical relation between Hg and biogenic materials is that the amount of algal material
287 during blooms is always large and therefore not a limiting factor for the scavenging of Hg. There has always been excess algal
288 material within or passing through the water column to scavenge all water column Hg. Thus, we assume that nearly all Hg in
289 the water column is removed through scavenging during diatom blooms, but that Hg scavenging events occur less frequently
290 during winter and summer/autumn seasons when primary productivity is lower and open ice expansion is at its maximum.
291 Similar to other elements, the periodic-like variations observed in the preindustrial Hg record. The influence of periodically
292 climatic changes of phytoplankton activity on periodical changes of Hg content was suggested before for the Caribbean Sea
293 (Kita et al., 2013). It is likely, that the periodic-like variations observed in the Adèlie Basin Hg record are also attributed to the

294 seasonal export of biological materials. There is also evidence, based on Hg levels in water (Canário et al. 2017) that relevant
295 to different development stages of a phytoplankton bloom, different amounts of dissolved Hg can be taken up by
296 phytoplankton. However, investigation at seasonal resolution is needed to further confirm our observations and hypotheses.

4. Conclusions

298 Investigation of Antarctic biogenic bottom sediments revealed that biological productivity and related scavenging of water
299 phase Hg by rapidly sinking algae or algae-derived organic matter controlled preindustrial Hg accumulation in Adélie Basin,
300 Antarctica. Our study suggests that the periodic-like variations in total Hg concentrations and accumulation rates are likely
301 associated with the opening and closing of polynya and its related changes in biological productivity. Although the high Hg
302 accumulation in diatom ooze does not represent the Hg sedimentation process across all the world's oceans, our data shows
303 that Hg scavenging by algae or fast sinking algae-derived organic matter is a key process controlling the sequestration of Hg
304 in marine sediments; and therefore the marine biogeochemical cycle of Hg in general. This can be similar to the association
305 between very high benthic organic C fluxes with diatom production at the surface water which can be accelerated by
306 aggregation (Sachs et al., 2009).

307 Our observations also suggest that re-emission of Hg from ocean surface waters as a result of reduction of Hg (II) might be
308 reduced due to Hg scavenging by algae, at least in areas of high primary productivity ecosystems comparable to Adélie Basin
309 ecosystem setup. Moreover, Hg fluxes to marine sediments might be higher than previously assumed in global model
310 estimations. More data from marine sediments is needed to support this assumption. A future increase in marine productivity
311 including algae blooms especially in coastal areas and semi-closed shallow seas will likely increase the Hg flux to bottom
312 sediments. The model study of Soerensen et al. (2016) for the Baltic Sea might serve as an example for changes in marine Hg
313 cycling caused by eutrophication. The area of the seafloor which is covered by remains of calcareous phytoplankton needs to
314 be considered in future studies as well owing to the role of calcareous species on Hg content (Kita et al., 2013).

315

316 *Author contributions.* S. Zaferani carried out the analyses. H. Biester planned the study and supervised the findings of this
317 work. The manuscript is written by both authors.

318 *Competing interests.* The authors declare that they have no conflict of interest

319 *Acknowledgments.* This research was supported by TU Braunschweig. We thank P. Schmidt and A. Calean for technical
320 assistance, Dr. DS. McLagan for the constructive comments on the manuscript.

References

Aksentov, K. I. and Sattarova, V. V.: Mercury geochemistry of deep-sea sediment cores from the Kuril area, northwest Pacific, Prog. Oceanogr., 180, 102235, doi:10.1016/j.pocean.2019.102235, 2020.

Amos, H. M., Jacob, D. J., Streets, D. G. and Sunderland, E. M.: Legacy impacts of all-time anthropogenic emissions on the global mercury cycle, Global Biogeochem. Cycles, 27, 410–421, https://doi.org/10.1002/gbc.20040, 2013.

Amyot, M., Gill, G. A. and Morel, F. M. M.: Production and loss of dissolved gaseous mercury in coastal seawater, Environ. Sci. Technol., 31(12), 3606–3611, doi:10.1021/es9703685, 1997.

Arrigo, K. R., Worthen, D., Schnell, A. and Lizotte, M. P.: Primary production in Southern Ocean waters, J. Geophys. Res. Ocean., 103, 15587–15600, https://doi.org/10.1029/98JC00930, 1998.

Canário, J., Santos-Echeandia, J., Padeiro, A., Amaro, E., Strass, V., Klaas, C., Hoppema, M., Ossebaar, S., Koch, B. P. and Laglera, L. M.: Mercury and methylmercury in the Atlantic sector of the Southern Ocean, Deep. Res. Part II Top. Stud. Oceanogr., 138, 52–62, doi:10.1016/j.dsr2.2016.07.012, 2017.

Cheburkin, A. K. and Shotyk, W.: An energy-dispersive miniprobe multielement analyzer (EMMA) for direct analysis of Pb and other trace elements in peats, Fresenius. J. Anal. Chem., 354, 688–691, https://doi.org/10.1007/s0021663540688, 1996.

Chen, S.-Y., Ambe, S., Takematsu, N. and Ambe, F.: The chemical states of iron in marine sediments by means of Mössbauer spectroscopy in combination with chemical leachings, J. Oceanogr., 52, 705–715, https://doi.org/10.1007/BF02239461, 1996.

Cossa, D., Heimbu, L., Lannuzel, D., Rintoul, S. R., Butler, E. C. V, Bowie, A. R., Averty, B., Watson, R. J. and Remenyi, T.: Mercury in the Southern Ocean, Geochim. Cosmochim. Acta, 75, 4037–4052, https://doi.org/10.1016/j.gca.2011.05.001, 2011.

Crosta, X., Romero, O., Armand, L. K. and Pichon, J.-J.: The biogeography of major diatom taxa in Southern Ocean sediments: 2. Open ocean related species, Palaeogeogr. Palaeoclimatol. Palaeoecol., 223, 66–92, https://doi.org/10.1016/j.palaeo.2005.02.015, 2005.

Crosta, X., Debret, M., Denis, D., Courty, M. and Ther, O.: Holocene long-and short-term climate changes off Adélie Land, East Antarctica, Geochemistry, Geophys. Geosystems, 8(11), 1–15, doi:https://doi.org/10.1029/2007GC001718, 2007.

Croudace, I. W. and Rothwell, R. G.: Micro-XRF Studies of Sediment Cores: Applications of a non-destructive tool for the environmental sciences, Springer., 2015.

Denis, D., Crosta, X., Zaragosi, S., Romero, O., Martin, B. and Mas, V.: Seasonal and subseasonal climate changes recorded in laminated diatom ooze sediments, Adelie Land, East Antarctica, The Holocene, 16, 1137–1147, https://doi.org/10.1177%2F0959683606069414, 2006.

Driscoll, C. T., Mason, R. P., Chan, H. M., Jacob, D. J. and Pirrone, N.: Mercury as a global pollutant: Sources, pathways, and effects, Environ. Sci. Technol., 47, 4967–4983, https://doi.org/10.1021/es305071v, 2013.

Escutia, C., Brinkhuis, H., Klaus, A. and Scientists, E. 318: Site U1357, Proc. Integr. Ocean Drill. Programprogr., 318, doi:10.2204/iodp.proc.318.105.2011, 2011.

353 Kita, I., Kojima, M., Hasegawa, H., Chiyonobu, S. and Sato, T.: Mercury content as a new indicator of ocean stratification and
354 primary productivity in Quaternary sediments off Bahama Bank in the Caribbean Sea, Quat. Res., 80(3), 606–613,
355 doi:10.1016/j.yqres.2013.08.006, 2013.

356 Le Faucheur, S., Campbell, P. G., Fortin, C. and Slaveykova, V. I.: Interactions between mercury and phytoplankton:
357 speciation, bioavailability, and internal handling, Environ. Toxicol. Chem., 33, 1211–1224, https://doi.org/10.1002/etc.2424,
358 2014.

359 Fowler, S. W. and Knauer, G. A.: Role of large particles in the transport of elements and organic compounds through the
360 oceanic water column, Prog. Oceanogr., 16(3), 147–194, doi:10.1016/0079-6611(86)90032-7, 1986.

361 Fitzgerald, W. F., Gill, G. A. and Kim, J. P.: An equatorial Pacific Ocean source of atmospheric mercury, Science (80-.).,
362 224(4649), 597–599, doi:10.1126/science.224.4649.597, 1984.

363 Fitzgerald, W. F., Lamborg, C. H. and Hammerschmidt, C. R.: Marine biogeochemical cycling of mercury, Chem. Rev., 107,
364 641–662, https://doi.org/10.1021/cr050353m, 2007.

365 Fütterer, D. K.: The solid phase of marine sediments, in: Marine geochemistry, edited by H. D. Schulz and M. Zabel, pp. 1–
366 25, Springer, Berlin, Heidelberg, https://doi.org/10.1007/978-3-662-04242-7_1%0A, 2006.

367 Horowitz, H. M., Jacob, D. J., Zhang, Y., DIbble, T. S., Slemr, F., Amos, H. M., Schmidt, J. A., Corbitt, E. S., Marais, E. A.
368 and Sunderland, E. M.: A new mechanism for atmospheric mercury redox chemistry: implications for the global mercury
369 budget, Atmos. Chem. Phys., 17, 6353–6371, https://doi.org/10.5194/acp-17-6353-2017, 2017.

370 Jansen, J., Hill, N. A., Dunstan, P. K., McKinlay, J., Sumner, M. D., Post, A. L., Eléaume, M. P., Armand, L. K., Warnock, J.
371 P., Galton-Fenzi, B. K. and Johnson, C. R.: Abundance and richness of key Antarctic seafloor fauna correlates with modelled
372 food availability, Nat. Ecol. Evol., 2, 71–80, https://doi.org/10.1038/s41559-017-0392-3, 2018.

373 Lamborg, C., Bowman, K., Hammerschmidt, C., Gilmour, C., Munson, K., Selin, N. and Tseng, C.-M.: Mercury in the
374 Anthropocene Ocean, Oceanography, 27, 76–87, https://doi.org/10.5670/oceanog.2014.11, 2014a.

375 Lamborg, C. H., Fitzgerald, W. F., O'Donnell, J. and Torgersen, T.: A non-steady-state compartmental model of global-scale
376 mercury biogeochemistry with interhemispheric atmospheric gradients, Geochim. Cosmochim. Acta, 66, 1105–1118,
377 https://doi.org/10.1016/S0016-7037(01)00841-9, 2002.

378 Lamborg, C. H., Hammerschmidt, C. R., Bowman, K. L., Swarr, G. J., Munson, K. M., Ohnemus, D. C., Lam, P. J.,
379 Heimbürger, L., Rijkenberg, M. J. A. and Saito, M. A.: A global ocean inventory of anthropogenic mercury based on water
380 column measurements, Nature, 512, 65–68, https://doi.org/10.1038/nature13563, 2014b.

381 Lamborg, C. H., Hammerschmidt, C. R. and Bowman, K. L.: An examination of the role of particles in oceanic mercury
382 cycling, Philos. Trans. R. Soc. A Math. Phys. Eng. Sci., 374, 20150297, https://doi.org/10.1098/rsta.2015.0297, 2016.

383 Leri, A. C., Mayer, L. M., Thornton, K. R., Northrup, P. A., Dunigan, M. R., Ness, K. J. and Gellis, A. B.: A marine sink for
384 chlorine in natural organic matter, Nat. Geosci., 8, 620–624, https://doi.org/10.1038/ngeo2481, 2015.

385 Lohan, M. C. and Tagliabue, A.: Oceanic micronutrients: trace metals that are essential for marine life, Elements, 14, 385–
386 390, https://doi.org/10.2138/gselements.14.6.385, 2018.

387 Mason, R. and Fitzgerald, W. F.: The distribution and biogeochemical cycling of mercury in the equatorial Pacific Ocean,
388 Deep Sea Res. Part I Oceanogr. Res. Pap., 40(9), 1897–1924, doi:10.1016/0967-0637(93)90037-4, 1993.

389 Mason, R., Rolfhus, K. R. and Fitzgerald, W. F.: Methylated and elemental mercury cycling in surface and deep ocean waters
390 of the North Atlantic, Water, Air, Soil Pollut., 80(1–4), 665–677, doi:10.1007/BF01189719, 1995.

391 Mason, R., Lawson, N. M. and Sheu, G. R.: Mercury in the atlantic ocean: Factors controlling air-sea exchange of mercury
392 and its distribution in the upper waters, Deep. Res. Part II Top. Stud. Oceanogr., 48(13), 2829–2853, doi:10.1016/S0967-
393 0645(01)00020-0, 2001.

394 Mason, R. and Sheu, G.-R.: Role of the ocean in the global mercury cycle, Global Biogeochem. Cycles, 16, 1–14,
395 https://doi.org/10.1029/2001GB001440, 2002.

396 Mason, R. P., Fitzgerald, W. F. and Morel, F. M.: The biogeochemical cycling of elemental mercury: anthropogenic influences,
397 Geochim. Cosmochim. Acta, 58, 3191–3198, https://doi.org/10.1016/0016-7037(94)90046-9, 1994.

398 Mason, R. P., Reinfelder, J. R. and Morel, F. M.: Uptake , Toxicity , and Trophic Transfer of Mercury in a Coastal Diatom,
399 Environ. Sci. Technol., 30, 1835–1845, https://doi.org/10.1021/es950373d, 1996.

400 Mason, R. P., Choi, A. L., Fitzgerald, W. F., Hammerschmidt, Chad R Lamborg, C. H., Soerensen, A. L. and Sunderland, E.
401 M.: Mercury biogeochemical cycling in the ocean and policy implications, Environ. Res., 119, 101–117,
402 https://doi.org/10.1016/j.envres.2012.03.013, 2012.

403 Michel, C., Gosselin, M. and Nozais, C.: Preferential sinking export of biogenic silica during the spring and summer in the
404 North Water Polynya (northern Baffin Bay): Temperature or biological control?, J. Geophys. Res. Ocean., 107(7), 1–1,
405 doi:10.1029/2000jc000408, 2002.

406 Moran, S. and Moore, R.: Kinetics of the removal of dissolved aluminum by diatoms in seawater: A comparison with thorium,
407 Geochim. Cosmochim. Acta, 56, 3365–3374, https://doi.org/10.1016/0016-7037(92)90384-U, 1992.

408 Morel, F. M. and Price, N.: The biogeochemical cycles of trace metals in the oceans, Science, 300, 944–947,
409 https://doi.org/10.1126/science.1083545, 2003.

410 Morel, F. M. M., Reinfelder, J. R., Roberts, S. B., Chamberlain, C. P., Lee, J. G. and Yee, D.: Zinc and carbon co-limitation
411 of marine phytoplankton, Nature, 369, 740–742, https://doi.org/10.1038/369740a0, 1994.

412 Nerentorp Mastromonaco, M. G., Gårdfeldt, K. and Langer, S.: Mercury flux over West Antarctic Seas during winter, spring
413 and summer, Mar. Chem., 193, 44–54, doi:10.1016/j.marchem.2016.08.005, 2017a.

414 Nerentorp Mastromonaco, M. G., Gårdfeldt, K., Assmann, K. M., Langer, S., Delali, T., Shlyapnikov, Y. M., Zivkovic, I. and
415 Horvat, M.: Speciation of mercury in the waters of the Weddell, Amundsen and Ross Seas (Southern Ocean), Mar. Chem.,
416 193, 20–33, doi:10.1016/j.marchem.2017.03.001, 2017b.

417 O'Driscoll, N. J., Siciliano, S. D., Lean, D. R. S. and Amyot, M.: Gross photoreduction kinetics of mercury in temperate
418 freshwater lakes and rivers: Application to a general model of DGM dynamics, Environ. Sci. Technol., 40(3), 837–843,
419 doi:10.1021/es051062y, 2006.

420 Pilskaln, C. H., Manganini, S. J., Trull, T. W., Armand, L., Howard, W., Asper, V. L. and Massom, R.: Geochemical particle
421 fluxes in the Southern Indian Ocean seasonal ice zone: Prydz Bay region, East Antarctica, Deep. Res. Part I Oceanogr. Res.
422 Pap., 51(2), 307–332, doi:10.1016/j.dsr.2003.10.010, 2004.

423 Qureshi, A., O'Driscoll, N. J., Macleod, M., Neuhold, Y. M. and Hungerbühler, K.: Photoreactions of mercury in surface
424 ocean water: Gross reaction kinetics and possible pathways, Environ. Sci. Technol., 44(2), 644–649, doi:10.1021/es9012728,
425 2010.

426 Rolfhus, K. R. and Fitzgerald, W. F.: Mechanisms and temporal variability of dissolved gaseous mercury production in coastal
427 seawater, Mar. Chem., 90(1-4 SPEC. ISS.), 125–136, doi:10.1016/j.marchem.2004.03.012, 2004.

428 Sachs, O., Sauter, E. J., Schlüter, M., Rutgers van der Loeff, M. M., Jerosch, K. and Holby, O.: Benthic organic carbon flux
429 and oxygen penetration reflect different plankton provinces in the Southern Ocean, Deep. Res. Part I Oceanogr. Res. Pap., 56,
430 1319–1335, https://doi.org/10.1016/j.dsr.2009.02.003, 2009.

431 Schartup, A. T., Thackray, C. P., Qureshi, A., Dassuncao, C., Gillespie, K., Hanke, A. and Sunderland, E. M.: Climate change
432 and overfishing increase neurotoxicant in marine predators, Nature, 572, 648–650, https://doi.org/10.1038/s41586-019-1468-
433 9, 2019.

434 Schlesinger, W. H. and Bernhardt, E. S.: The Oceans, in: Biogeochemistry: an analysis of global change, pp. 341–395,
435 Academic press., 2013.

436 Selin, N. E.: Global biogeochemical cycling of mercury: a review, Annu. Rev. Environ. Resour., 34, 43–63,
437 https://doi.org/10.1146/annurev.environ.051308.084314, 2009.

438 Shanks, A. L. and Trent, J. D.: Marine snow: microscale nutrient patches 1, Limnol. Oceanogr., 24, 850–854,
439 https://doi.org/10.4319/lo.1979.24.5.0850, 1979.

440 Smetacek, V., Klaas, C., Strass, V. H., Assmy, P., Montresor, M., Cisewski, B., Savoye, N., Webb, A., D'Ovidio, F., Arrieta,
441 J. M., Bathmann, U., Bellerby, R., Berg, G. M., Croot, P., Gonzalez, S., Henjes, J., Herndl, G. J., Hoffmann, L. J., Leach, H.,
442 Losch, M., Mills, M. M., Neill, C., Peeken, I., Röttgers, R., Sachs, O., Sauter, E., Schmidt, M. M., Schwarz, J., Terbrüggen,
443 A. and Wolf-Gladrow, D.: Deep carbon export from a Southern Ocean iron-fertilized diatom bloom, Nature, 487(7407), 313–
444 319, doi:10.1038/nature11229, 2012.

445 Soerensen, A. L., Schartup, A. T., Gustafsson, E., Gustafsson, B. G., Undeman, E. and Björn, E.: Eutrophication increases
446 phytoplankton methylmercury concentrations in a coastal sea - A Baltic sea case study, Environ. Sci. Technol., 50, 11787–
447 11796, https://doi.org/10.1021/acs.est.6b02717, 2016.

448 Soerensen, A. L., Mason, R., Balcom, P. H. and Sunderland, E. M.: Drivers of surface ocean mercury concentrations and air-
449 sea exchange in the West Atlantic Ocean, Environ. Sci. Technol., 47(14), 7757–7765, doi:10.1021/es401354q, 2013.

450 Soerensen, A. L., Mason, R., Balcom, P. H., Jacob, D. J., Zhang, Y., Kuss, J. and Sunderland, E. M.: Elemental mercury
451 concentrations and fluxes in the tropical atmosphere and Ocean, Environ. Sci. Technol., 48(19), 11312–11319,
452 doi:10.1021/es503109p, 2014.

453 Sunderland, E. M. and Mason, R. P.: Human impacts on open ocean mercury concentrations, Global Biogeochem. Cycles, 21,
454 1–15, https://doi.org/10.1029/2006GB002876, 2007.

455 Turner, J. T.: Zooplankton fecal pellets, marine snow, phytodetritus and the ocean's biological pump, Prog. Oceanogr., 130,
456 205–248, doi:10.1016/j.pocean.2014.08.005, 2015.

457 Vandal, G. M., Fitzgerald, W. F., Boutron, C. F. and Candelone, J.-P.: Variations in mercury deposition to Antarctica over the
458 past 34,000 years, Nature, 362, 621, https://doi.org/10.1038/362621a0, 1993.

459 Wang, J., Xie, Z., Wang, F. and Kang, H.: Gaseous elemental mercury in the marine boundary layer and air-sea flux in the
460 Southern Ocean in austral summer, Sci. Total Environ., 603, 510–518, doi:10.1016/j.scitotenv.2017.06.120, 2017.

461 Whalin, L., Kim, E. H. and Mason, R.: Factors influencing the oxidation, reduction, methylation and demethylation of mercury
462 species in coastal waters, Mar. Chem., 107(3), 278–294, doi:10.1016/j.marchem.2007.04.002, 2007.

463 Williams, G. D., Bindoff, N. L., Marsland, S. J. and Rintoul, S. R.: Formation and export of dense shelf water from the Adélie
464 depression, East Antarctica, J. Geophys. Res. Ocean., 113(4), 1–12, doi:10.1029/2007JC004346, 2008.

465 Yamane, M., Yokoyama, Y., Miyairi, Y., Suga, H., Matsuzaki, H., Dunbar, R. B. and Ohkouchi, N.: Compound-specific 14C
466 dating of IODP Expedition 318 core U1357A obtained off the Wilkes Land Coast, Antarctica, Radiocarbon, 56(3), 1009–1017,
467 2014.

468 Zaferani, S., Pérez-rodríguez, M. and Biester, H.: Diatom ooze—A large marine mercury sink, Science, 361, 797–800,
469 https://doi.org/10.1126/science.aat2735, 2018.

470

471 **Table 1: Factor loadings for the five significant components extracted by PCA from Adélie Basin sediment samples.**

Elements	Components				
	1	2	3	4	5
Mn	**0.89**	0.40	-0.05	-0.05	0.01
Ti	**0.89**	0.43	0.01	0.04	-0.02
Rb	**0.84**	0.03	0.39	0.10	0.20
Zr	**0.83**	-0.22	0.05	-0.15	0.08
K	**0.73**	**0.66**	0.05	0.08	0.10
Y	**0.73**	-0.34	0.10	-0.09	0.05
Al	0.12	**0.93**	0.06	0.05	0.18
Si	0.03	**0.84**	-0.28	-0.11	-0.28
S	0.01	**0.84**	0.16	0.12	0.26
Cl	-0.16	**0.76**	0.25	0.22	0.42
Zn	-0.05	0.15	**0.78**	0.15	0.11
Cu	0.31	0.03	**0.76**	0.31	0.21
Ni	0.11	-0.08	**0.75**	-0.10	0.00
Fe	**0.62**	0.03	**0.64**	0.20	0.19
Br	-0.23	0.35	**0.50**	0.46	0.48
Hg	0.17	0.09	-0.04	**0.79**	0.14
As	-0.01	-0.09	0.30	**0.73**	-0.26
Pb	0.35	-0.11	-0.10	**-0.62**	-0.18
Sr	0.25	0.09	0.37	0.16	**0.83**
Ca	0.22	**0.52**	-0.03	-0.13	**0.67**
Eigenvalue	6.62	3.95	3.34	1.35	0.98
% variance	33.1	19.7	16.7	6.7	4.9

472

473
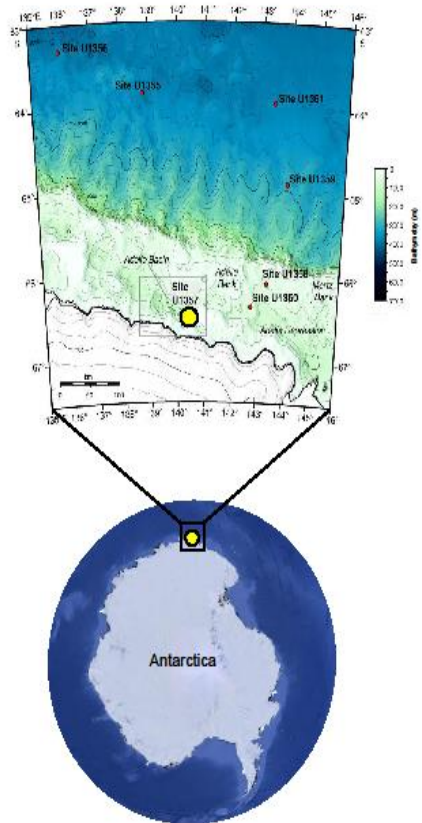
Figure 1: Location of the IODP318-U1357B core in the Adélie Basin, East Antarctica, indicated by a yellow dot (Antarctic
image source © Google Earth. Bathymetric map is reproduced from Escutia et al., 2011).
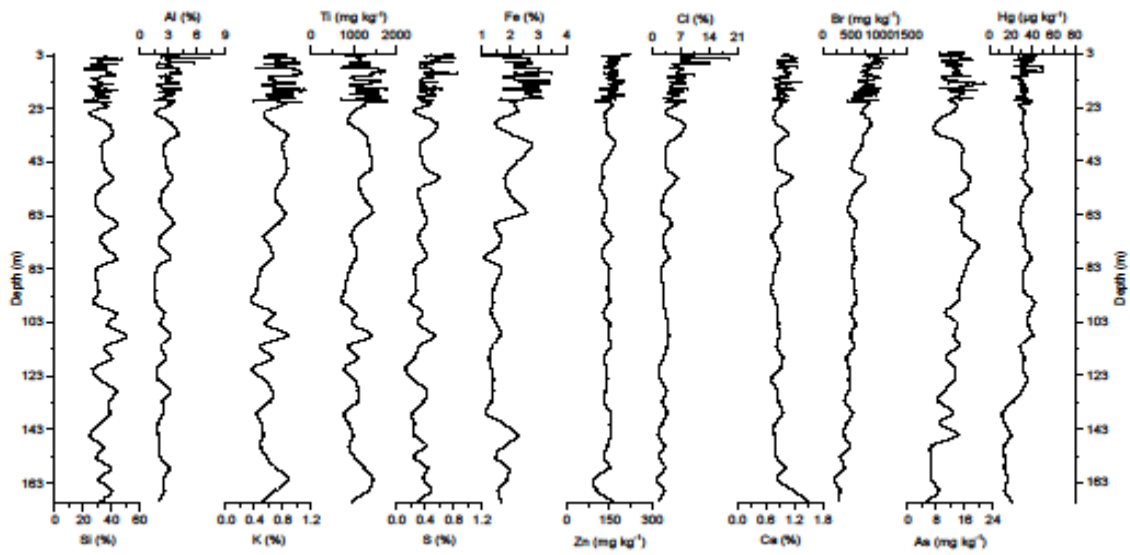
476

477   Figure 2: Down core records of Si, Al, K, Ti, S, Fe, Zn, Cl, Ca, Br, As, and Hg concentrations of Adélie Basin sediments.
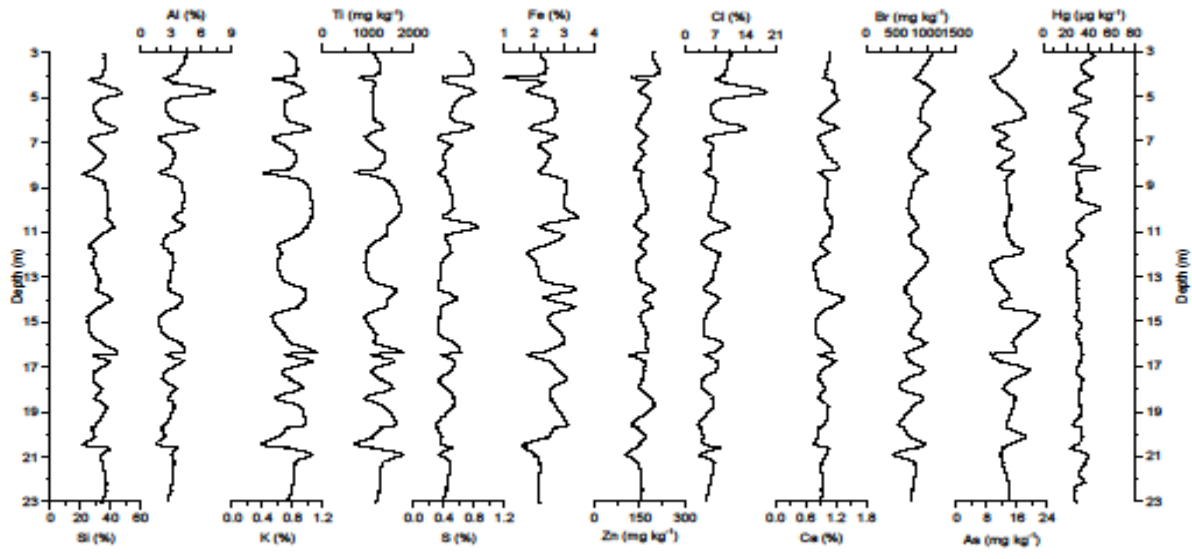
478

479   Figure 3: Down core records of Si, Al, K, Ti, S, Fe, Zn, Cl, Ca, Br, As, and Hg concentrations of Adélie Basin sediments for
480   the top 23 m of the core.
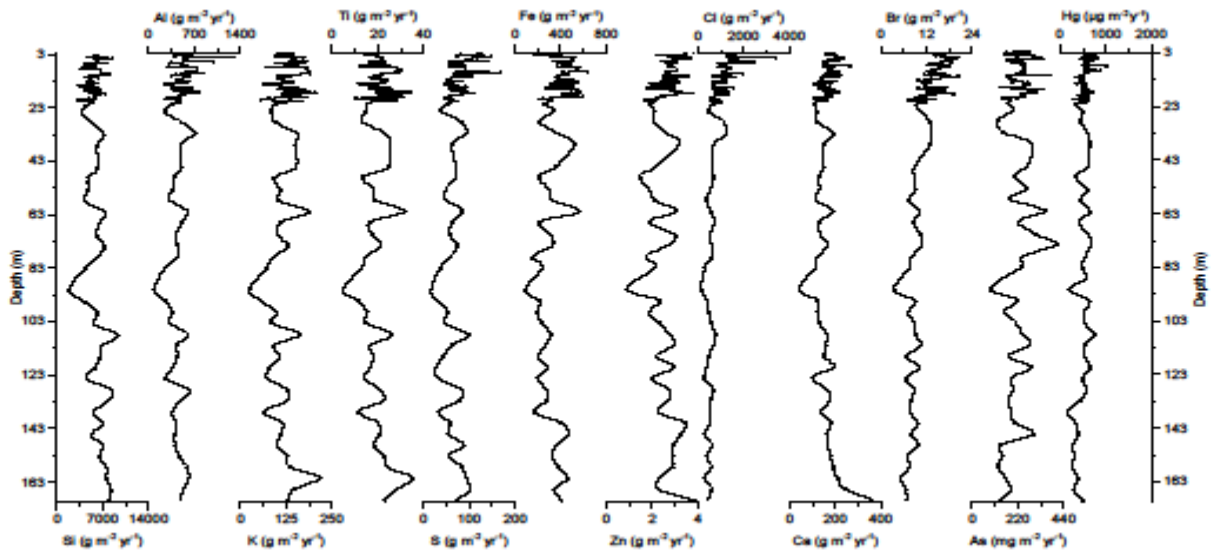
481

482   Figure 4: Down core records of Si, Al, K, Ti, S, Fe, Zn, Cl, Ca, Br, As, and Hg accumulation rates of Adélie Basin sediments.
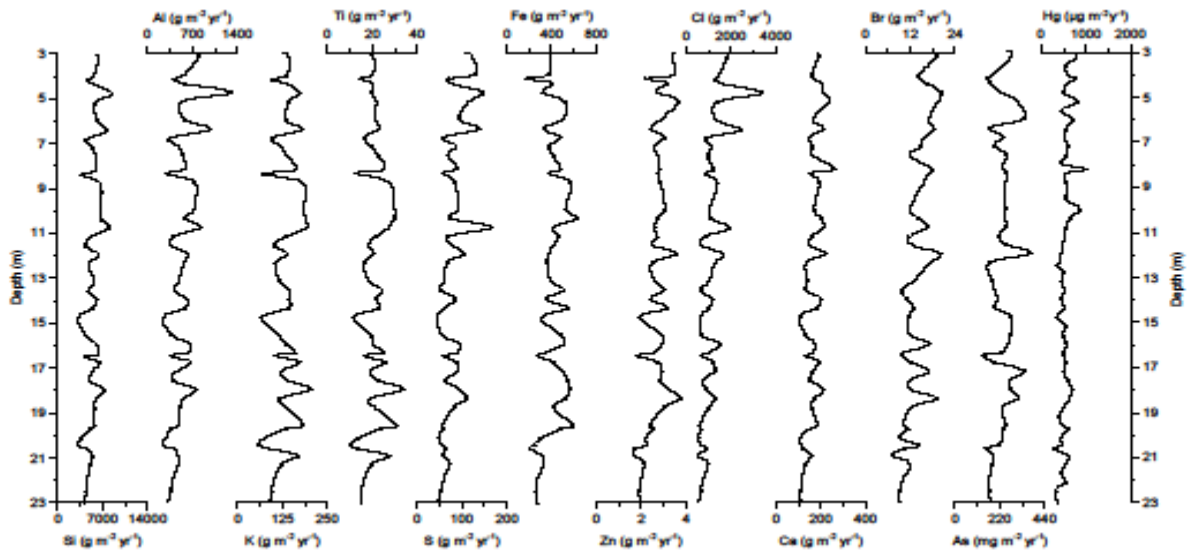
483

484 Figure 5: Down core records of Si, Al, K, Ti, S, Fe, Zn, Cl, Ca, Br, As, and Hg accumulation rates of Adélie Basin sediments
485 for the top 23 m of the core.
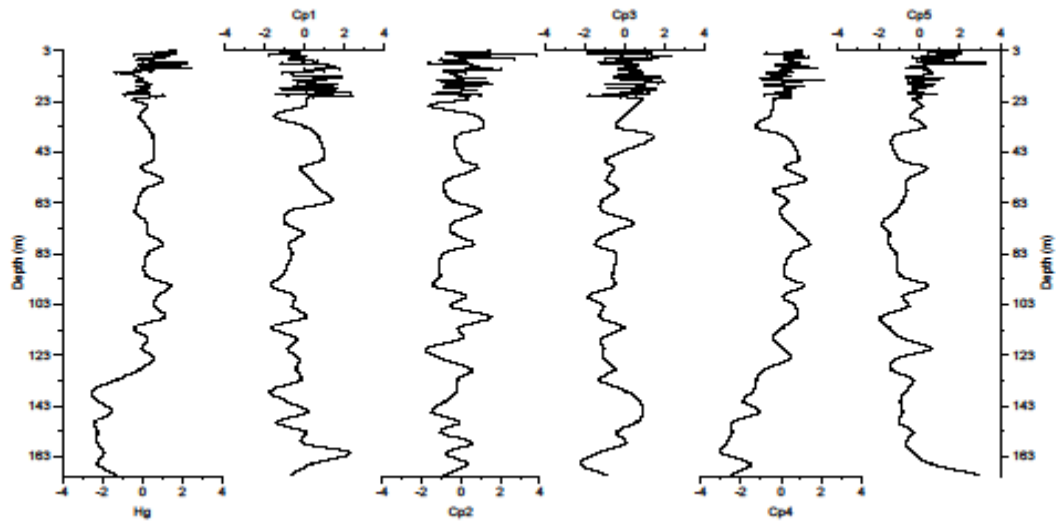
486

487 Figure 6: Depth records of scores of the principal components extracted by PCA on the elemental composition of the sediments
488 along with Z-score of Hg of the Adélie Basin sediments.
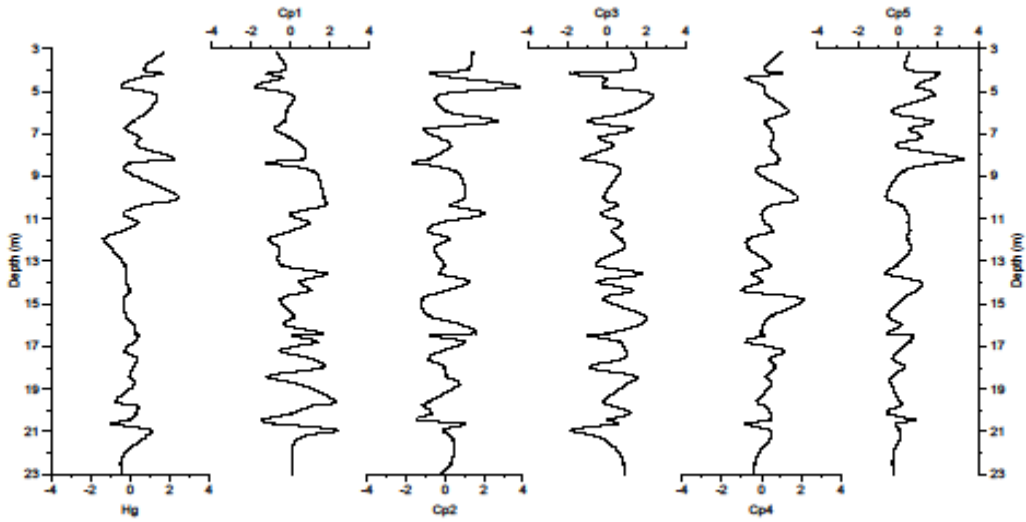
489

490   Figure 7: Depth records of scores of the principal components extracted by PCA on the elemental composition of the sediments
491   along with Z-score of Hg of the Adélie Basin sediments for the top 23 m of the core.
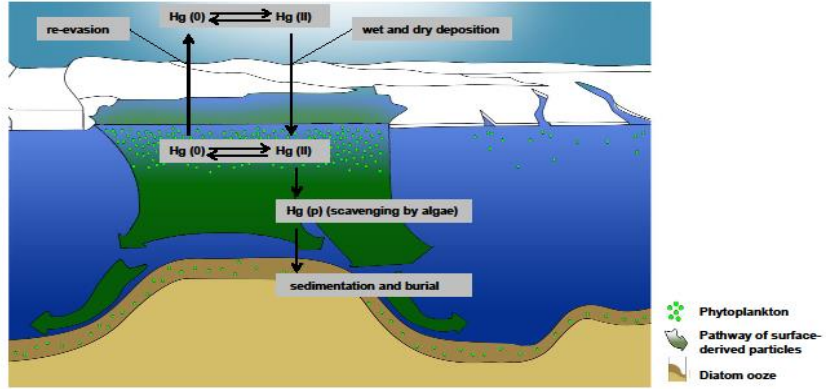
492

493 Figure 8: Adélie Basin schematic Hg cycle model indicating the processes controlling Hg deposition and accumulation under
494 high primary production. Fast-sinking diatom particles remove dissolved water phase Hg from the water column through
495 scavenging (Figure is adapted from Jansen et al., 2018).